Analysing the effect of temperature for steam fluidized-bed gasification of biomass with MP-PIC simulation

Janitha C. Bandara, Britt M. E. Moldestad, Marianne S. Eikeland

Faculty of Technology, Department of Natural Sciences and Maritime Sciences, University College of South-Eastern Norway, Kjølnes Ring 56, 3901, Porsgrunn, Norway.

Abstract
Gasification in fluidized beds is an outstanding technology in biomass to energy conversion. The multiphase particle-in-cell modelling has reduced the computational time related to CFD simulations of dense gas-solid systems like fluidized bed gasification. Barracuda VR commercial CFD package was used to analyse the effect of reactor temperature in steam gasification of biomass.
The product gas composition, lower heating value and the cold gas efficiency were compared for steam at 873K, 973K and 1073K. The steam-to-biomass ratio was maintained at a constant value of 0.45. The hydrogen content of the product gas changed from 36% to 57% as the temperature was increased from 873K to 1073K whereas the carbon monoxide content changed from 33% to 13%. The lower heating value and the cold gas efficiency changed from 10.4 MJ/kg to 10.1 MJ/kg and 76.6% to 73.2% respectively within the same temperature range. The formation of tar was not modelled and the gas composition showed high sensitivity towards the reactor temperature.

1. Introduction
Energy has been a key drive in human development where excessive consumption of fossil fuels have had negative impacts on the environment. Increased emissions of anthropogenic carbon dioxide from fossil fuel combustion has been identified as the root cause for the global warming and many of the subsequent phenomena. Renewable energy is important in replacing fossil fuels where biomass is the dominating source having 10% to 14% share of the global energy profile [1]. Lignocellulose is the leading bioenergy source, which is about 90% of the accessible biomass feedstock on earth [2]. Biochemical conversion of lignocellulosic materials into secondary fuels and chemicals is less interesting compared to thermochemical conversion, due to low carbon conversion and slow conversion rates. Combustion and co-combustion produce direct heat that can be used in heating applications or power generation. Pyrolysis and gasification products are used in either direct combustion or secondary fuel and chemical synthesis. Fluidized bed combustion and gasification are interested over fixed bed designing due to many inherent advantages. Enhanced gas-solid contact and intense mixing establish efficient heat and mass transfer that guarantees the homogeneous reactor temperature. This increases the possibility and reliability of scaled up operation. Proper control over solid particles, large thermal inertia of solids, increased efficiency, reduced

emissions and wide range of operating conditions are additional advantages of fluidized bed systems [3, 4]. Further, high mixing avoids the hot spot and cold spot generation in highly exothermic reactors. This feature is extremely important in biomass gasification as high temperatures leads to ash melting/agglomeration where reduced tar cracking and char conversion are resulted from low temperatures [5, 6].

1.1 Fluidized bed gasification of biomass

Gasification is an interesting process due to the versatility of the produced gas. Carbon monoxide (CO), hydrogen (H_2), carbon dioxide (CO_2), methane (CH_4), high molecular hydrocarbons (ethane etc.), condensable hydrocarbons (tar) and nitrogen (N_2) are the main components in the product gas where the unconverted char and ash are left in the sold residue [7]. Air is the most common gasifying agent and the lower heating value (LHV) of the product gas is low (4-7 MJ/Nm^3) with relatively low H_2 content of 8-14%. As the gas is diluted with N_2, it can only be used in heating applications or power generation industry. In contrast, the product gas from oxygen (O_2) or steam (H_2O) gasification has high LHV up to 18 MJ/Nm^3 with H_2 yield up to 60% [8, 9]. The product gas is then referred as "*synthesis gas*" which is possible to use in both power generation and as a feedstock for synthesis of secondary fuels or chemicals (bio-ethanol, synthesis diesel, methanol, bio-methane and H_2 etc.). The LHV is the crucial parameter for heat and power industries, while it is the carbon-to-hydrogen ratio for the synthesis of fuels and chemicals. Apart from many operational difficulties, tar in the product gas has been the major challenge of biomass gasification, which leads to clogging of pipes and catalyst poisoning. In many situations, the heating value and the tar content of the gas decides the product gas quality [7]. A simple pictorial representation of successive steps of biomass gasification is given in Figure 1. Drying and pyrolysis are the first steps where combustion and gasification reactions are responsible for the char and tar conversion into light gases. The total process is more complex with hundreds of reactions and most influencing reactions are listed in Table 2.
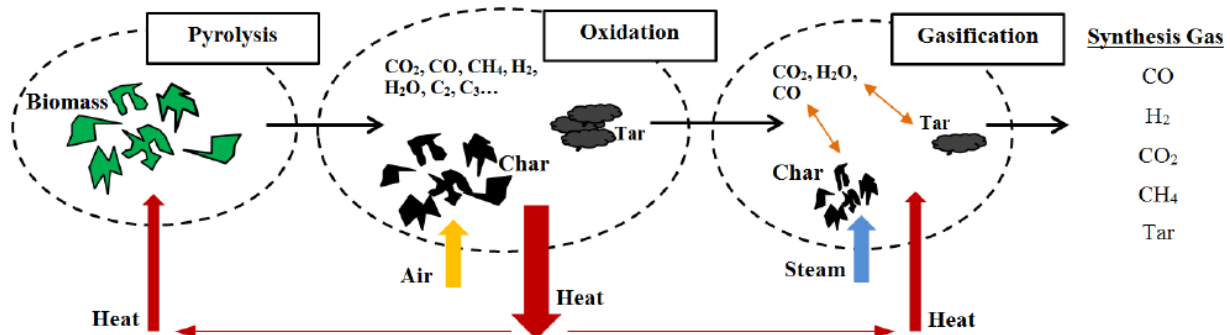

Figure 1. Biomass gasification process.

The complete gasification reaction is endothermic. Hence, it is necessary to supply that energy demand by combusting a fraction of the biomass internally or by external heating, which are distinguished as auto-thermal and allo-thermal gasification respectively. O_2 driven gasification is expensive and therefore, it is necessary to optimize the system between air and steam. As described above, N_2 dilution is the major drawback of the air gasification. Dual circulating fluidized bed (DCFB) gasification, as illustrated in Figure 2, is a better design in overcoming this challenge. A supporting bedding material such as sand particles is used, as the wood chips/pellets are hard to fluidize [10]. DCFB system separates the combustion reactions from the gasification and pyrolysis reactions. Biomass (chips or pellets) is fed into the gasification reactor, which is operated with steam. The biomass go through pyrolysis and gasification reactions to produce synthesis gas. The unreacted char flows down to the combustion reactor along with bed material. The combustion reactor is operated with air in which the bed material absorbs the heat generated from char combustion. The heated bed material is recycled back into the gasification reactor across a cyclone followed by a proper gas seal such as a loopseal. Hence, this combination of exothermal (combustion) and endothermal (gasification) reactors make the whole system an auto-thermal process [11]. Gasification reactor is typically operated in the bubbling fluidization regime, while the combustion reactor is in fast fluidization regime as a riser combustor [12]. This configuration eliminates the N_2 dilution of the product gas with additional advantages as discussed above [13]. Fluidized catalytic cracking (FCC) makes the early

remarks of this configuration where Corella et al [11] have discussed different configurations of dual fluidized bed systems.

Lv et al [9] has carried out experimental studies of steam gasification in a fluidized bed reactor and observed increased carbon conversion, gas yield and H_2 content at elevated temperatures. In contrast, the LHV was observed to become lower at higher temperature. Xiao et al [14] has also done experimental studies in a DCFB gasification system and observed similar results of higher H_2 content with increased temperature. Pfeifer, Koppatz and Hofbauer [15, 16] have carried out detailed experiments of biomass gasification in a DCFB system where the product gas composition was analysed as a function of temperature, bed material and fuel moisture.
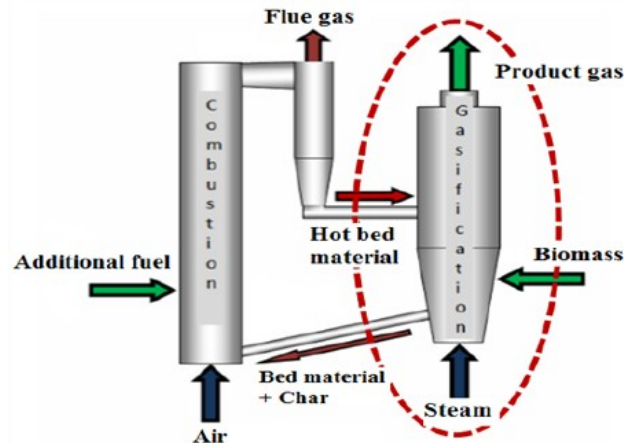

Figure 2. Schematic diagram of dual circulating fluidized bed gasification.

1.2 CFD simulation of fluidized bed gasification

Experimental optimization of fluidized bed gasification is rather challenging and difficult (i.e. optimization of geometry, biomass-feeding location etc.). Computational fluid dynamic (CFD) simulations of three-dimensional geometries in real scale have become realistic with the improved computer power and efficient numerical algorithms. Hence, CFD simulation is a useful tool to analyse the effects of operational conditions such as temperature, pressure, steam-to-biomass ratio (S/B), equivalence ratio (ER) etc. in fluidized bed gasification [17]. The behaviour of different biomass feedstock, particle sizes, flow patterns, geometry etc. can also be analysed with respect to the product gas quality including gas composition and lower heating value (LHV).

CFD is a highly proven technique for single-phase systems where the predictions agree well against the most accurate measurement apparatus [18]. However, CFD modelling and simulation of multiphase systems is challenging due to the additional weights imposed from the dispersed phase (solid particles, liquid droplets etc.) properties. Modelling of momentum exchange between phases, inter particle forces such as electrostatic, van der Waals forces, inter-particle collision and variation in size, shape and density in solid phase are some of the challenges [18]. Additional terms for particle heating, pyrolysis, gas combustion and heterogeneous reactions are involved in fluidized bed gasification. Above all, the dimensional scale differences between the reactor and the particles make the CFD modelling even more challenging [19].

Multiphase CFD models can be broadly distinguished as Eulerian-Eulerian or Eulerian-Lagrangian. In Eulerian-Eulerian modelling, both phases are modelled with Navier Stokes equations considering interpenetrating continua. This approach is referred as two-fluid model, which has been dominating in modelling of dense phase systems over many years due to its less demand of computer power. The discrete nature of particles is not captured in Eulerian modelling while the particle phase properties are approximated with kinetic theory of granular flow (KTGF). Modelling of particle mixtures is difficult, as it is necessary to define a separate phase for each size, shape or density in the mixture. In contrast, Lagrangian modelling of particle phase preserves the discrete nature where each particle is modelled by equations of Newton's law of motion [19]. However, this approach is computationally expensive and limited to 2×10^5 number of particles [20]. The multiphase particle-in-cell (MP PIC) technique is an extended version of the Lagrangian modeling which overcome certain limitations of conventional implementation.

In MP-PIC modeling, the fluid phase is modeled in the Eulerian grid with Navier Stokes equations. Particles having similar characteristics, such as size, shape and density are grouped, which are referred as either parcels or computational particles. Hence, billions of particles could be encapsulated into millions of computational particles and modelled in the Lagrangian approach [21]. Inter particle stresses are calculated in the Eulerian grid considering the particles as a continuum and these values are mapped back to the individual particles, using interpolation functions [22]. It has been found that the required quantity of parcels to model the particle phase accurately is acceptable and makes it possible to simulate large-scale particle systems.

The Barracuda VR commercial package is specially developed for multiphase CFD simulations, which uses the MP-PIC approach. This novel approach is named as computational particle fluid dynamics (CPFD). Solnordal et al [23] and Liang & Zhang [24] have carried out MP-PIC simulations for bubbling fluidized beds. Snider et al [25] have presented the integration of heat and reaction chemistry in MP-PIC simulations whereas Loha et al [26] and Xie et al [27] have published simulations of bubbling fluidized bed gasification. Liu, Cattolica & Seiser [28, 29] have performed MP-PIC simulations for a complete DCFB gasifier system. The ability of defining multi-component particles is a distinctive feature of Barracuda, which facilitates the integration of devolatization reactions involved in gasification and combustion.

CPFD simulation of a complete DCFB gasification system is complex in generating the computational grid and expensive in simulation time. The main objective of this work was to analyse the effect of the temperature in steam gasification. Therefore, only the gasification reactor of a DCFB system (as highlighted in Figure 2) was simulated with Barracuda VR 17.0.3 version where the particle temperature from the combustion reactor was assumed.

2. MP PIC model equations

The subscripts "g", "p" and "i" represent the gas phase, particle phase and species respectively. The gas phase mass and momentum conservation is given by continuity and time averaged Navier-Stokes equations those are respectively represented in equation 1 and 2.

$$\frac{\partial(\alpha_g\rho_g)}{\partial t} + \nabla.\left(\alpha_g\rho_g u_g\right) = \delta\dot{m}_p \tag{1}$$

$$\frac{\partial(\alpha_g\rho_g u_g)}{\partial t} + \nabla.\left(\alpha_g\rho_g u_g u_g\right) = -\nabla P + F + \nabla.\left(\alpha_g\tau_g\right) + \alpha_g\rho_g g \tag{2}$$

α, ρ and u represent volume fraction, density and velocity respectively. $\delta\dot{m}_p$ in equation 1 is the mass production from gas-solid reactions. P stands for pressure and F represents the interface momentum transfer. The gas phase stress tensor τ_g is given by equation 3,

$$\tau_g = \mu_g\left[\left(\nabla u_g + \Delta u_g^T\right) - \frac{2}{3}\nabla.u_g I\right] \tag{3}$$

μ_g refers to the shear viscosity that is the sum of the laminar and turbulent components. The large eddy simulation is used for the large-scale turbulence modeling while the subgrid scale turbulence is captured with Smagorinsky model as given in equation 4,

$$\mu_{g,t} = C_s\rho_g\Delta^2\left|\nabla u_g + \Delta u_g^T\right| \tag{4}$$

Where Δ is the subgrid length scale and calculated by equation 5. The default value for the model constant C_s is 0.01.

$$\Delta = (\delta x\delta y\delta z)^{1/3} \tag{5}$$

The energy conservation of gas phase is given by,

$$\frac{\partial(\alpha_g\rho_g h_g)}{\partial t} + \nabla.\left(\alpha_g\rho_g h_g u_g\right) = \alpha_g\left(\frac{\partial P}{\partial t} + u_g.\nabla P\right) + \emptyset - \nabla.\left(\alpha_g q\right) + \dot{Q} + S_h + \dot{q}_D \tag{6}$$

The enthalpy is represented by h. The viscous dissipation $\emptyset$ and the energy source per volume $\dot{Q}$ were ignored in this work. S_h is the conservative energy exchange from particle phase to gas phase. $\dot{q}_D$ is the enthalpy diffusion term and q is the gas heat flux.

$$q = \lambda_g \nabla T_g \tag{7}$$

$$\dot{q}_D = \sum_{i=1}^{N} \nabla \cdot \left(h_i \alpha_g \rho_g D \nabla Y_{g,i} \right) \tag{8}$$

Where, λ is the thermal conductivity calculated by molecular conductivity (λ_m) and eddy conductivity λ_t from Reynolds stress mixing theory. The Prandlt (Pr) number, which is calculated from $c_p \mu_t / \lambda_t$ was set as 0.9. D denotes the turbulent mass diffusivity, which is correlated to the viscosity by Schmidt number (Sc) and given by $Sc = \mu / \rho_g D$. The value of the Sc was taken as 0.9. Y represents the species mass fraction. The gas and species enthalpies are calculated from,

$$h_g = \sum_{i=1}^{N} Y_{g,i} h_i \tag{9}$$

$$h_i = \int_{T_o}^{T_g} C_{p,i} dT + \Delta h_{f,i} \tag{10}$$

$\Delta h_{f,i}$ is the formation enthalpy of species "i" at reference temperature of T_o. C_p is the specific heat capacity. The pressure is calculated from the equation of state for the ideal gas,

$$P = \rho_g R T_g \sum_{i=1}^{N} \frac{Y_{g,i}}{MW_i} \tag{11}$$

R is the universal gas constant and the MW refers to the molecular weight of the species. As the gas phase is composed with mixture of gases, transport equation is solved for each species. The transport equation for the each species in the gas phase is given by,

$$\frac{\partial(\alpha_g \rho_g Y_{g,i})}{\partial t} + \nabla \left(\alpha_g \rho_g Y_{g,i} u_g \right) = \nabla \cdot \left(\rho_g D \alpha_g \nabla Y_{g,i} \right) + \delta m_{i,chem} \tag{12}$$

D denotes the turbulent mass diffusivity where $\delta m_{i,chem}$ represents the net production of species due to gas phase chemical reactions.
The interface momentum transfer is calculated by the viscous drag force as given in equation 06,

$$F = \iint f \left\{ m_p \left[D_p (u_g - u_p) - \frac{\nabla P}{\rho_p} \right] \right\} dm_p du_p \tag{13}$$

The particle dynamics are formulated with particle distribution function (PSD), which is calculated from Liouville equation.

$$\frac{\partial f_p}{\partial t} + \nabla(f_p u_p) + \nabla u_p(f_p A_p) = \frac{f_D - f_p}{\tau_D} \tag{14}$$

f_p is a function of spatial location, velocity, mass and temperature of particles and the time. Therefore $\iiint (f_p) du_p dm_p dT_p$ is the average number of particles per unit volume with velocities, mass and temperatures in the intervals of $(u_p, u_p + du_p)$, $(m_p, m_p + dm_p)$ and $(T_p, T_p + dT_p)$. f_D is the particle distribution function for the local mass averaged particle velocity and τ_D is the particle collision damping time.
Where the particle trajectory and acceleration are given by,

$$u_p = \frac{\partial(x_p)}{\partial t} \quad and \quad A_p = \frac{\partial(u_p)}{\partial t} = D_p(u_g - u_p) - \frac{\nabla P}{\rho_p} - \frac{\nabla \tau_p}{\rho_p \alpha_p} + g + F_p \tag{15}$$

The particle volume fraction of the above equation is given by,

$$\alpha_p = \iint f \frac{m_p}{\rho_p} dm_p du_p \tag{16}$$

Particle interactions are modeled with the particle stress function developed by Harris and Crighton,

$$\tau_p = \frac{10 P_s \alpha_p^\beta}{max[(\alpha_{cp} - \alpha_p), \varepsilon(1 - \alpha_p)]} \tag{17}$$

3. Barracuda CFD setup

A previously validated CPFD hydrodynamic model developed by the authors was used in this work [30]. The Wen-Yu-Ergun drag correlation was used with 40% momentum retention for particle collision. It was necessary to activate the blended acceleration model as the particle mixture was composed with different densities and sizes. The restitution coefficients for the particle-wall collision were 0.3 and 0.99 for normal and tangential directions respectively. Default values of 1, 3 and 10^{-8} were used for P_s, β and ε respectively in particle stress function (equation 17).

The reactor was a 2000 mm high cylindrical column with a diameter of 550 mm in. The computational grid, boundary conditions and the initial particle filling are illustrated in Figure 3.
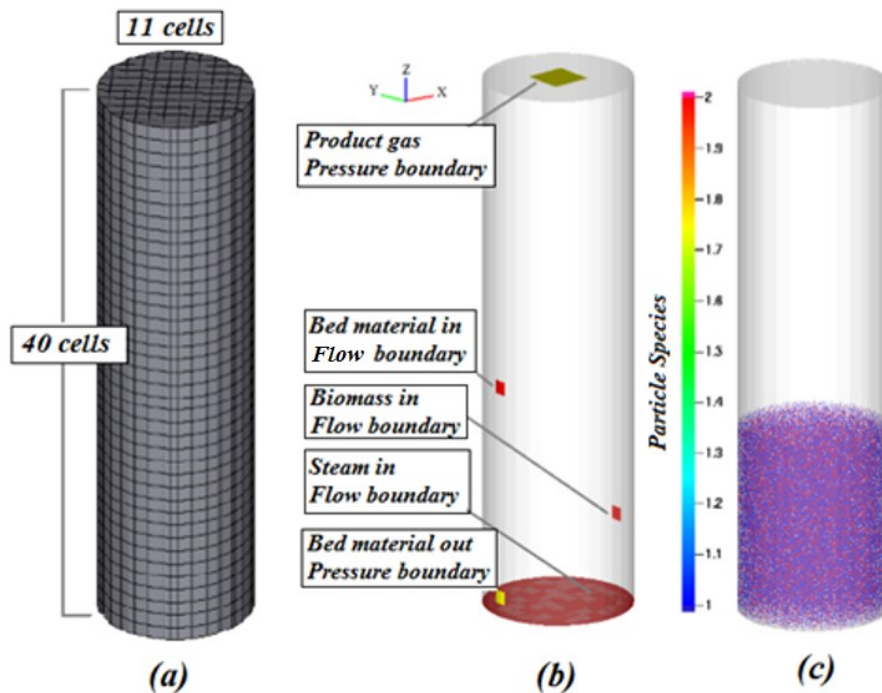

Figure 3. (a) Computational grid, (b) Boundary conditions, (c) Initial particle filling of sand, char and biomass.

Table 1 contains the rest of the operational and physical parameters used in the simulation. Uniform grid option was used and there were 4840 computational cells in the geometry. Uniform steam distribution was assumed without a distributor plate at the bottom flow boundary. Hot bed material from the combustion reactor was assumed free of char and 200K higher than the steam temperature. In Barracuda, particle inflows should be assisted by a fluid stream and the fluid inflow volume can be adjusted by manipulating the "slip velocity" option. The bed material outflow from the reactor bottom was implemented as a pressure boundary where the flowrate was adjusted by changing the pressure of that particular cell. The bed material outflow and hot bed material inflow was connected via "particle feed control" option. A pressure boundary at the reactor top was defined for the produced gas to escape and "*no particle exit*" option was applied to inhibit the particle outflow. Thermal wall option was not used and therefore, the system was consisted with adiabatic walls.

Steam at 1073 K, 973 and 873 K were used to analyze the system behavior. The initial reactor temperature was set to the respective steam temperature as it takes a substantial time for particle heating from the room

temperature. It was intended to keep the steam-to-biomass ratio at a constant value of 0.45 for all the simulations. Similarly, the steam velocity was also intended to keep at a constant value as it affects the gas residence time and the bed hydrodynamics. However, even with the constant steam velocity of 0.47 m/s, the steam mass flowrates in to the reactor changed due to the varying density resulted from the temperature change. Therefore, it was necessary to change the biomass flowrates accordingly to keep the constant S/B ratio of 0.45. Detailed information about boundary conditions and initial conditions for 1073 K steam temperature are given in Table 01. The biomass flowrates were changed to 0.055 kg/s and 0.06 kg/s at 973 K and 873 K respectively. The Arrhenius reaction rate models were used in the homogeneous and heterogeneous reactions. The constants of the reaction models were adapted from Thapa et al [31] and are tabulated in Table 2.

Table 1. Initial and boundary conditions.

Boundary Conditions			
Stream	**Boundary**	**Parameters**	**Particle**
Steam	Flow	1073K, 101325Pa, 0.47m/s	Nil
Product gas	Pressure	101325pa	Nil
Biomass in	Flow	400K, 101325Pa, 0.5m/s	0.05 kg/s
Bed material in	Flow	1273K, 101325Pa, 0.25m/s	95% bed material out
Bed material out	Pressure	100000pa	Particle outflow
Initial Conditions			
Fluid	1073 K, 101325 Pa, steam, total volume		
Silica	1073 K, 101325 Pa, 1000 µm, spherical, 0.48 volume fraction, density 2200 kg/m³, 600 mm height initial fill		
Char	1073 K, 101325 Pa, 500 µm, spherical, 0.12 volume fraction, density 300 kg/m³, 600 mm height initial fill		

Table 2. Reaction Kinetics.

Reaction		Reaction Rate Kinetics	Enthalpy
$C + H_2O \leftrightarrow H_2 + CO$	Forward	$1.272 m_s\, T\, exp\left[\dfrac{-22645}{T}\right][H_2O]$	+131 kJ/mole
(steam Gasification)	Reverse	$1.044 * 10^{-4}\, m_s\, T^2 exp\left[\dfrac{-6319}{T} - 17.29\right][H_2][CO]$	
$C + CO_2 \leftrightarrow 2CO$	Forward	$1.272 m_s\, T\, exp\left[\dfrac{-22645}{T}\right][CO_2]$	+172 kJ/mole
(Boudouard reaction)	Reverse	$1.044 * 10^{-4}\, m_s\, T^2 exp\left[\dfrac{-2363}{T} - 20.92\right][CO]^2$	
$0.5C + H_2 \leftrightarrow 0.5CH_4$	Forward	$1.368 * 10^{-3}\, m_s\, T\, exp\left[\dfrac{-8078}{T} - 7.087\right][H_2]$	-75 kJ/mole
(Methanation)	Reverse	$0.151\, m_s\, T^{0.5} exp\left[\dfrac{-13578}{T} - 0.372\right][CH_4]^{0.5}$	
$H_2O + CO \leftrightarrow H_2 + CO_2$	Forward	$7.68 * 10^{10}\, m_s\, T\, exp\left[\dfrac{-36640}{T}\right][CO]^{0.5}[H_2O]$	-41 kJ/mole
(Water-gas-shift)	Reverse	$6.4 * 10^9\, m_s\, T\, exp\left[\dfrac{-39260}{T}\right][H_2]^{0.5}[CO_2]$	
$CH_4 + H_2O \leftrightarrow 3H_2 + CO$	Forward	$3.0 * 10^5\, T\, exp\left[\dfrac{-15042}{T}\right][CH_4][H_2O]$	+206 kJ/mole
(Methane reforming)	Reverse	$0.0265\, T\, exp\left[\dfrac{-32900}{T}\right][CO][H_2]^2$	
Pyrolysis	Forward	$264000\, m_s\, \theta_f\, exp\left[\dfrac{-12629}{T}\right]$	

Following the literature data, the char and volatile fractions of biomass were assumed as 25% and 75% respectively with no moisture and ash. Formation of tar and higher molecular hydrocarbons were neglected where only H_2, CO, CO_2, CH_4 and H_2O were assumed to evolve from pyrolysis. Weight fractions of CH_4, CO, CO_2 and H_2 in the pyrolysis gas were taken as 0.1213, 0.6856, 0.1764 and 0.0167 respectively [31].

4. Results and discussion

Simulations were carried out for 100 seconds and the gas composition, the gas temperature and the particle mass flow rates were monitored. As mentioned in the introduction, the combustion reactor was not modelled in this work. Instead, temperature of the bed material flowing from the combustion reactor was assumed as 200 K higher than that of the respective reactor temperature. Then, the bed material inlet temperatures were 1273, 1173 and1073 K for 1073, 973 and 873 K reactor temperatures respectively. Average gas composition was read as the time average over final 25 seconds of the simulation. A detailed description of the simulation results for 1073K steam temperature is presented in section 3.1 while the rest of the content elaborates the comparison of results between different temperatures.

4.1 Simulation results of 1073 K steam temperature

Being a continuous reactor system, the bed mass was supposed to be constant over time. However, a slight reduction of bed mass from 178.3 kg to 177.1 kg was observed over 100s of simulation time. Bed particle outflow was also monitored and the plots in Figure 4 depict the variation of total solid and char flowrates.
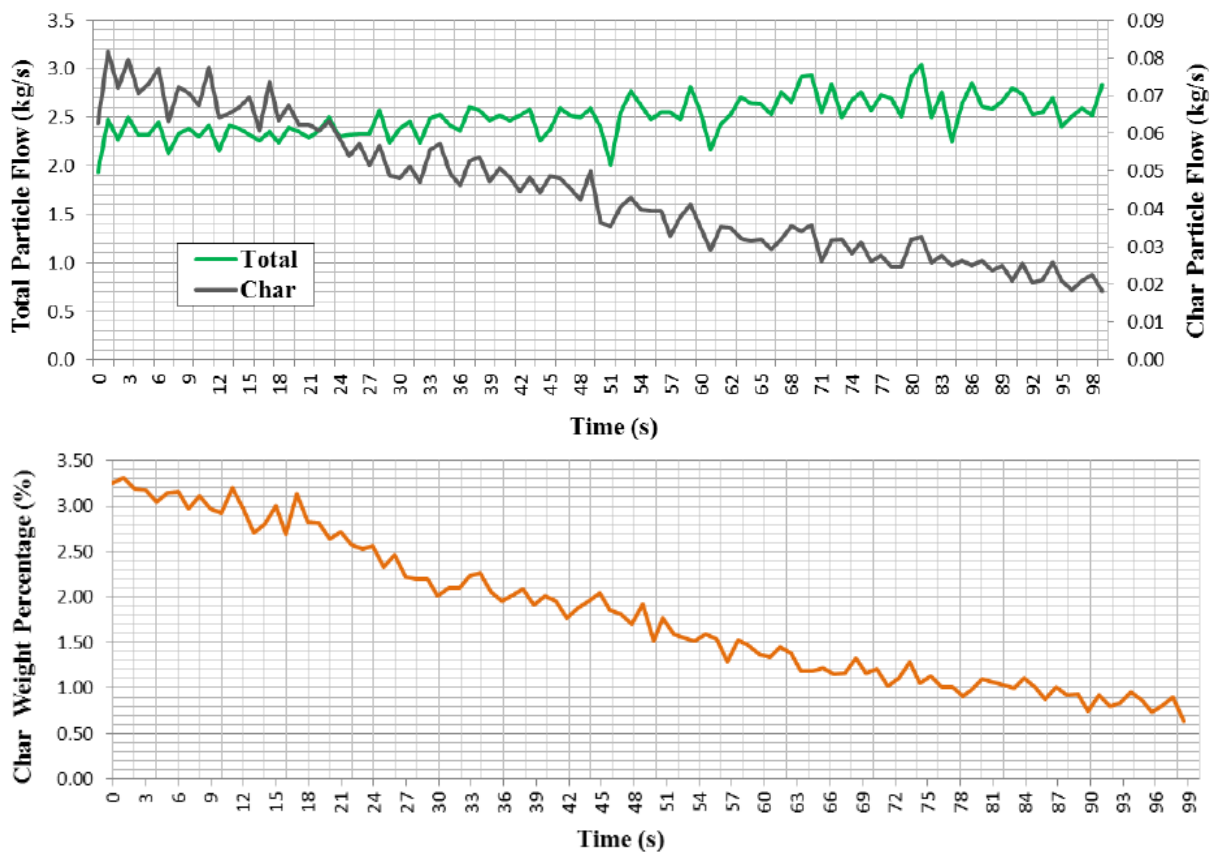

Figure 4. Total solid & char flowrate (up) and char percentage of particle outflow (down).

According to the Figure 4, the char percentage in the particle outflow has got reduced from 3.25% to 0.5%. If the perfect mixing conditions are assumed, char percentage inside the reactor and in the particle outflow should be identical. Therefore, char inventory in the reactor has got reduced simultaneously. Further, the particle outflow was connected to the bed material inlet with 99% efficiency (assuming 1% of char in the particle outflow which undergoes oxidation in the combusttion reactor). Hence, the reduction of char inventory in the reactor and innefficient implementation of the boundary connection might lead to the reduction of total material inventory in the reactor. It can be further concluded that the initial char

percentage in the reactor is much higher than the equlibrium char content with the implemented biomass flow of 0.05 kg/s.

As the bed hydrodynamics are concerned, it was desired the column to operate in the bubbling fluidization regime with homogeneous temperature and particle species distribution. Particular parameters are illustrated in Figure 5. Sketch (c) in Figure 5 refers to the distribution of different particle species in the reactor where 1, 2, and 3 represents silica, char and biomass respectively. Sketch (a) clearly depicts that the reactor is operated in the bubbling fluidization regime with a slight particle entrainment in the freeboard. When the sketch (a) and (c) are analysed together, it is clearly illustrated that the entrained fraction consists of biomass particles. The bed temperature shows a slight uneven distribution as shown in sketch (b). However, the particle bed has reached higher temperatures than 1073 K, which was the steam inlet temperature and desired reactor temperature. The pyrolysis reactions and char conversion reactions are endothermic, which absorb the heat from the bed material. The plot (b) in Figure 7 shows that the gas temperature has increased continuously over the simulation time, which suggests the possibility of reducing either the particle circulation rate or the temperature from the combustion reactor. Temperature rise of bed material in the combustion reactor was assumed and it would have been more realistic if the complete reactor system (with both reactors) was simulated. According to the Figure 5 (c), the particle species of silica, char and biomass are finely distributed over the reactor, which is a proper indication of good mixing with less segregation.
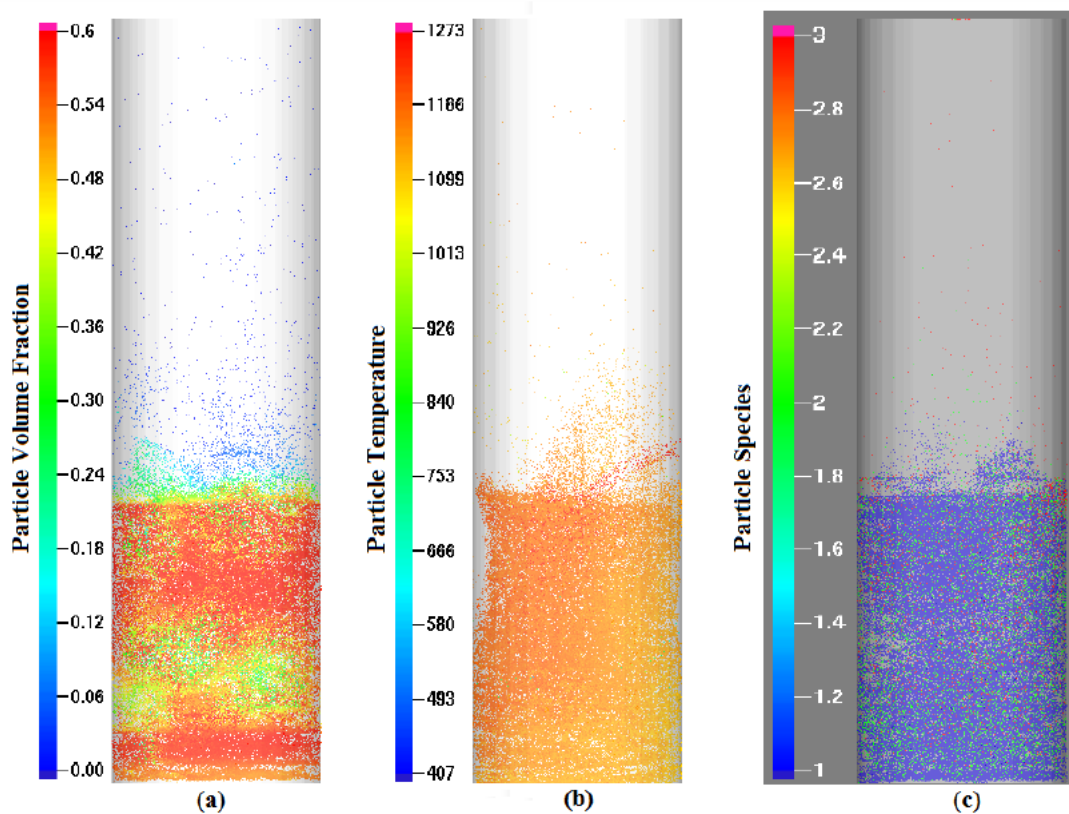

Figure 5. Bed hydrodynamics at 100 s simulation time, (a) Particle volume fractions, (b) Particle temperature distribution, and (c) Particle species distribution (1- sand, 2-char and 3-biomass).

The product gas composition was monitored over the reactor height and the simulation time as illustrated in Figure 6 and Figure 7(a) respectively. Temperature and flowrate of the product gas against the time are plotted in Figure 7(b) and (c). Gas composition does not show noticeable variations up to biomass feeding height of 300mm from the bottom of the reactor. This suggests slow reaction kinetics of the steam-char heterogeneous reaction at reactor temperature. Carbon monoxide is the main constituent in the biomass pyrolysis gas, which is approximately 68%. However, due to the fast kinetics of water-gas-shift reaction, CO is immediately consumed and concentrations drop sharply. The increasing H_2 and CO_2 concentration along the reactor height with simultaneous reduction of CO describes the dominance of the water-gas-shift reaction.
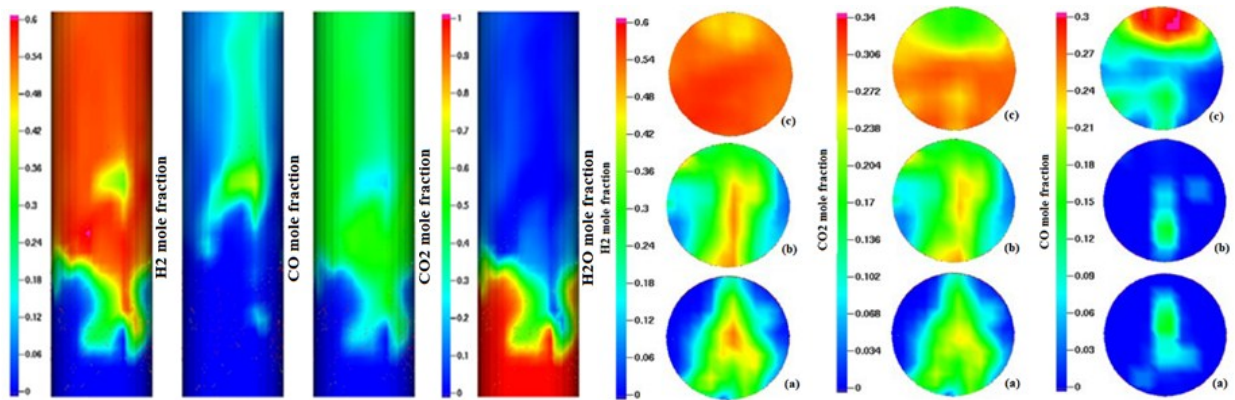
Figure 6. Gas composition along reactor height (left), different cross sections (right), (a) 0.3m, (b) 0.6m and (c), 0.9m.
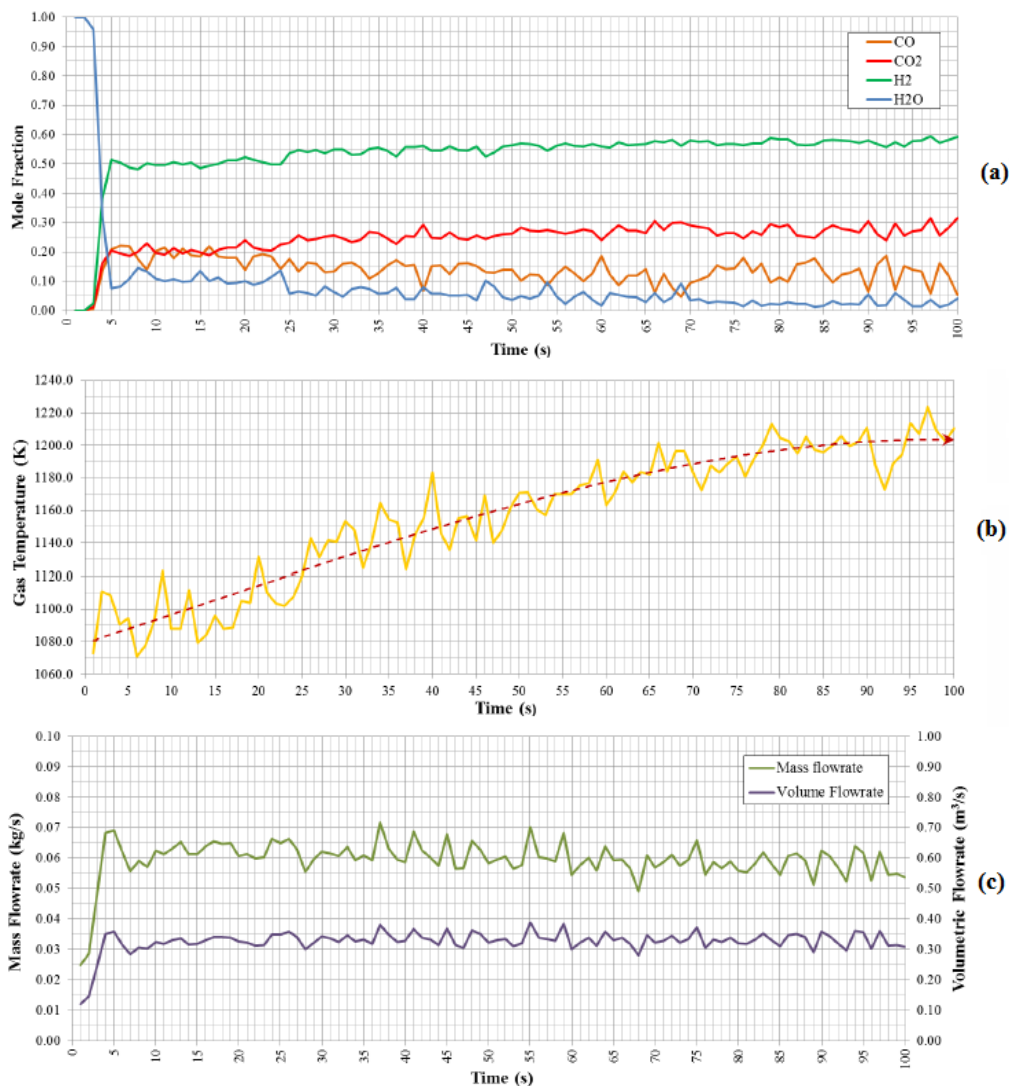

Figure 7. Product gas properties over simulation time, (a) Composition, (b) Temperature (c) Flowrate.

According to Figure 7(a), the system has reached nearly steady state operation in 5 seconds. However, there is a gradual change in the gas compositions with the time. H_2 mole fraction has changed from 0.5 to 0.6 between 5s and 100s, which analogues to the increasing gas temperature. At elevated temperatures, the reaction kinetics are increased and the system reaches the equilibrium state rapidly.

The mass and area specific mass production rates of gas were 0.055 kg/s and 0.23 kg/s/m² respectively. As the produced gas was at high temperatures and atmospheric pressure, the ideal gas low was applied to

reproduce the data at normal temperature and pressure (25 °C and 1 atm). The product gas flowrate was 1.64 Nm³/kg of biomass, which is within the range found in literature. Further, area specific gas production was calculated as 0.34 Nm³/s/m². The average molar gas composition during final 25s simulation was 0.128 of CO, 0.273 of CO_2, 0.574 of H_2 and 0.025 of H_2O. The LHV of the gas was calculated as 10.1 MJ/kg taking LHV of wood, CO and H_2 as 16 MJ/kg (dry basis), 10 MJ/kg and 120 MJ/kg respectively. The cold gas efficiency (CGE) was calculated as 73.3% using following equation,

$$CGE = \frac{mass_{gas}(kg)}{mass_{fuel}(kg)} \frac{LHV_{gas}(J/kg)}{LHV_{fuel}(J/kg)} \tag{18}$$

There is a certain level of uncertainty related to calculation of cold gas efficiency because, the actual operating conditions of the combustion reactor was not known. Instead, the temperature increase of the bed material in the combustion reactor was assumed as 200K. However, there can be additional fuel supply into the combustion to achieve the aforementioned temperature rise, which indirectly affects the cold gas efficiency.

4.2 Effect of the temperature

The effect of the steam temperature on the product gas was analysed by simulating the same reactor at 973K and 873K temperatures. The temperature increment in the combustion reactor was assumed as 200K, similar to previous case. The time taken to achieve the near steady state conditions got increased as the steam temperature was reduced. The respective times were 7s and 10s to achieve the steady state conditions at 973K and 873K. Further, as illustrated in Figure 3(b), the outlet pressure boundary was defined as a small fraction of the top face of the reactor cylinder. Consequently, it was assumed that the cross sectional variation of the gas composition is averaged out and it is agreeable to represent the gas composition by the centre cell of the outlet pressure boundary. It simply works as a sensor installed at the place of that particular cell. Figures 8, 9 depict the average gas composition at three different temperatures considered.
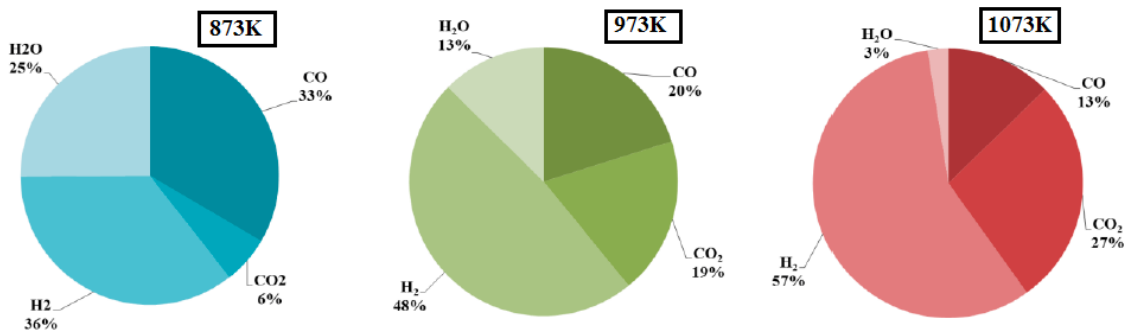

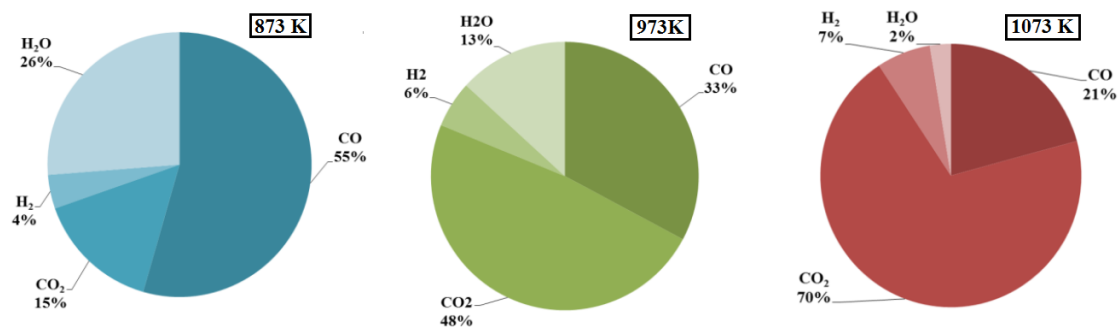Figure 8. Product gas composition (molar basis) at different temperatures.

Figure 9. Product gas composition (weight basis) at different temperatures.

Even though the S/B was constant at 0.45 for all the simulations, it was required to change the biomass flowrate accordingly with the varied steam flow due to the temperature change. Therefore, the comparison of the effect of temperature is not 100% representative. However, it is clear that the water-gas-shift reaction dominates over the gas composition. At the temperature of 873K, 25 mole% of the gas is composed of un-reacted steam. The steam content reduced to 13 mole% and 3 mole% when the temperature was increased to 973K and 1073K respectively. Simultaneous increment of H_2 and CO_2 along with reduction of H_2O and

CO analogue to increased temperature is a clear indication of triggered chemical kinetics at high temperatures. Therefore, when it comes to 873K and 973K reactor temperature, the gas composition can be improved by providing higher residence time by increasing the reactor height. However, the simulation results from the reactor operation at 1073K show that almost all the steam has been consumed. Hence, it is necessary to increase the gas-solid contact and trigger the heterogeneous reaction between char and CO_2 to improve the gas quality. Reducing the biomass particle size and upgrading the reactor into fast fluidization regime are two possible methods in achieving increased gas-solid contact. Reduced particle size increases the contact surface area where, fast fluidization drives more particles into the freeboard increasing the contact time, which can finally be operated as a circulating fluidized bed. The plots in Figure 10 illustrate the change of gas composition in the reactor freeboard at 1073K and the summary of the simulation results at different temperatures are given in Table 3.
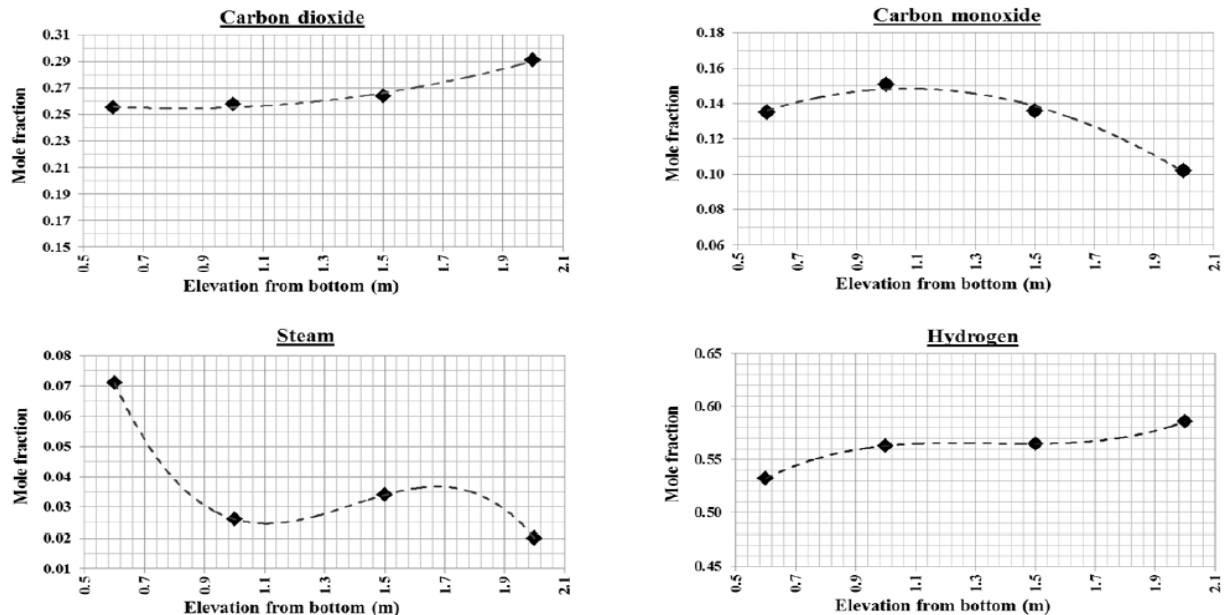

Figure 10. Change of gas composition along reactor freeboard at 1073 K.

Table 3. Simulation derived results at different temperatures.

Parameter	1073K	973K	873K
Steam flow (kg/s)	0.0228	0.0251	0.028
Gas temperature (K)	1200	1100	970
Volumetric gas Production (Nm^3/s)	0.082	0.091	0.1
Mass gas production (kg/s)	0.055	0.064	0.074
Volumetric gas production (Nm^3/kg biomass)	1.64	1.65	1.66
LHV (MJ/kg)	10.1	10.0	10.4
Cold gas efficiency (%)	73.2	73.4	76.6

The increased volumetric gas production at reduced temperature is due to the increased steam and biomass flowrates into the system. Further, gas production rate per unit mass of biomass has also increased. Both LHV and CGE have increased slightly with decreased temperature. In order to verify the facts further, an additional simulation was performed at 973K steam temperature with identical steam and biomass flowrates at 1073K. The steam velocity was reduced to 0.45 m/s to maintain the S/B ratio at 0.45. The LHV dropped from 10.1 MJ/kg at 1073K to 9.97 MJ/kg at 973K. In contrast, CGE increased from 73.2% to 76.52% within same temperature range. No significant variation in the gas composition was observed. The gas residence time increases with the reduced gas velocities and consequently, the system has additional time to reach the equilibrium.

5. Conclusion

Barracuda VR commercial CFD package was used in this work where MP-PIC implementation delivered fast results. This suggests its suitability in optimizing the reactor systems. The effect of steam and reactor temperature was analysed regard to gas composition, lower heating value of gas, gas flow rates and cold gas efficiency.

The hydrogen content in the product gas was directly proportional to the reactor temperature. The reaction kinetics are triggered because of the increased temperature that drives the system towards the equilibrium state faster. The carbon monoxide content showed a simultaneous reduction with increased temperature and hydrogen content, which is a clear illustration of the water-gas-shift reaction. Considerable amount of excess steam existed at operational temperatures of 973K and 873K. The underlying reasons can be due to either the changed equilibrium compositions or inadequate residence time, which should be further analysed by increasing the reactor height. The lower heating value of the product gas was not strongly correlated to temperature, which changed from 10.1 MJ/kg to 10.4 MJ/kg as the temperature was changed from 1073K to 873K. There was a slight increment in the cold gas efficiency at reduced temperature from 73.2% at 1073K to 76.6% at 873K. In brief, the gas composition was a strong function of the system temperature while the lower heating value and cold gas efficiency showed only little variations.

The effect of the temperature difference was not 100% illustrative with the applied implementation of boundary conditions. Therefore, it is recommended to keep all other parameters constant except temperature, in order to picture the exact effect of temperature for product gas quality. Simulating the complete dual fluidized bed reactor system together with a detailed characterization of biomass such as composition and pyrolysis kinetics, will overcome the uncertainties related to this work for a certain extent.

Acknowledgements

References

[1]   REN21, "Renewables 2016 Global Status Report," 2016.

[2]   J. Szczodrak and J. Fiedurek, "Technology for conversion of lignocellulosic biomass to ethanol," Biomass and Bioenergy, vol. 10, no. 5, pp. 367-375, 1996.

[3]   E. Esmaili and N. Mahinpey, "Adjustment of drag coefficient correlations in three dimensional CFD simulation of gas–solid bubbling fluidized bed," Advances in Engineering Software, vol. 42, no. 6, pp. 375-386, 2011.

[4]   F. Winter and B. Schratzer, "23 - Applications of fluidized bed technology in processes other than combustion and gasification A2 - Scala, Fabrizio," in Fluidized Bed Technologies for Near-Zero Emission Combustion and Gasification: Woodhead Publishing, 2013, pp. 1005-1033.

[5]   Y. Behjat, S. Shahhosseini, and S. H. Hashemabadi, "CFD modeling of hydrodynamic and heat transfer in fluidized bed reactors" Int. Comm. in Heat and Mass Transfer, 35(3), 357-368, 2008.

[6]   M. Horio, "1 - Overview of fluidization science and fluidized bed technologies A2 - Scala, Fabrizio," in Fluidized Bed Technologies for Near-Zero Emission Combustion and Gasification: Woodhead Publishing, 2013, pp. 3-41.

[7]   A. A. P. Susastriawan, H. Saptoadi, and Purnomo, "Small-scale downdraft gasifiers for biomass gasification: A review," Renewable and Sustainable Energy Reviews, vol. 76, pp. 989-1003, 2017.

[8]   X. T. Li, J. R. Grace, C. J. Lim, A. P. Watkinson, H. P. Chen, and J. R. Kim, "Biomass gasification in a circulating fluidized bed," Biomass and Bioenergy, vol. 26, no. 2, pp. 171-193, 2004.

[9]   P. M. Lv, Z. H. Xiong, J. Chang, C. Z. Wu, Y. Chen, and J. X. Zhu, "An experimental study on biomass air–steam gasification in a fluidized bed" Bioresource Technology, 95 (1), 95-101, 2004.

[10]   H. Cui and J. R. Grace, "Fluidization of biomass particles: A review of experimental multiphase flow aspects," Chemical Engineering Science, vol. 62, no. 1, pp. 45-55, 2007.

[11]   J. Corella, J. M. Toledo, and G. Molina, "A Review on Dual Fluidized-Bed Biomass Gasifiers," Industrial & Engineering Chemistry Research, vol. 46, no. 21, pp. 6831-6839, 2007.

[12]   G. Xu, T. Murakami, T. Suda, Y. Matsuzaw, and H. Tani, "Two-stage dual fluidized bed gasification: Its conception and application to biomass" Fuel Processing Tech. 90(1), 137-144, 2009.

[13]   T. Murakami, G. Xu, T. Suda, Y. Matsuzawa, H. Tani, and T. Fujimori, "Some process fundamentals of biomass gasification in dual fluidized bed," Fuel, vol. 86, no. 1, pp. 244-255, 2007.

[14]   Y. Xiao, S. Xu, Y. Song, Y. Shan, C. Wang, and G. Wang, "Biomass steam gasification for hydrogen-rich gas production in a decoupled dual loop gasification system," Fuel Processing Technology, vol. 165, pp. 54-61, 2017.

[15]   C. Pfeifer, S. Koppatz, and H. Hofbauer, "Steam gasification of various feedstocks at a dual fluidised bed gasifier: Impacts of operation conditions and bed materials," Biomass Conversion and Biorefinery, journal article vol. 1, no. 1, pp. 39-53, 2011.

[16] S. Koppatz, C. Pfeifer, and H. Hofbauer, "Comparison of the performance behaviour of silica sand and olivine in a dual fluidised bed reactor system for steam gasification of biomass at pilot plant scale," Chemical Engineering Journal, vol. 175, pp. 468-483, 2011.

[17] M. Chiesa, V. Mathiesen, J. A. Melheim, and B. Halvorsen, "Numerical simulation of particulate flow by the Eulerian–Lagrangian and the Eulerian–Eulerian approach with application to a fluidized bed," Computers & Chemical Engineering, vol. 29, no. 2, pp. 291-304, 2005.

[18] J. R. Grace and F. Taghipour, "Verification and validation of CFD models and dynamic similarity for fluidized beds," Powder Technology, vol. 139, no. 2, pp. 99-110, 2004.

[19] X. Ku, T. Li, and T. Løvås, "CFD–DEM simulation of biomass gasification with steam in a fluidized bed reactor," Chemical Engineering Science, vol. 122, pp. 270-283, 2015.

[20] D. Gidaspow, J. Jung, and R. K. Singh, "Hydrodynamics of fluidization using kinetic theory: an emerging paradigm," Powder Technology, vol. 148, no. 2, pp. 123-141, 2004.

[21] M. J. Andrews and P. J. O'Rourke, "The multiphase particle-in-cell (MP-PIC) method for dense particulate flows," International Journal of Multiphase Flow, vol. 22, no. 2, pp. 379-402, 1996.

[22] D. M. Snider, "An Incompressible Three-Dimensional Multiphase Particle-in-Cell Model for Dense Particle Flows," Journal of Computational Physics, vol. 170, no. 2, pp. 523-549, 2001.

[23] C. B. Solnordal, V. Kenche, T. D. Hadley, Y. Feng, P. J. Witt, and K. S. Lim, "Simulation of an internally circulating fluidized bed using a multiphase particle-in-cell method," Powder Tech. 274, 123-134, 2015.

[24] Y. Liang, Y. Zhang, T. Li, and C. Lu, "A critical validation study on CPFD model in simulating gas–solid bubbling fluidized beds," Powder Technology, vol. 263, pp. 121-134, 2014.

[25] D. M. Snider, S. M. Clark, and P. J. O'Rourke, "Eulerian–Lagrangian method for three-dimensional thermal reacting flow with application to coal gasifiers," Chem. Eng. Sc., 66 (6), 1285-1295, 2011.

[26] C. Loha, H. Chattopadhyay, and P. K. Chatterjee, "Three dimensional kinetic modeling of fluidized bed biomass gasification," Chemical Engineering Science, vol. 109, pp. 53-64, 2014.

[27] J. Xie, W. Zhong, B. Jin, Y. Shao, and H. Liu, "Simulation on gasification of forestry residues in fluidized beds by Eulerian–Lagrangian approach," Bioresource Technology, 121, pp. 36-46, 2012.

[28] H. Liu, R. J. Cattolica, and R. Seiser, "CFD studies on biomass gasification in a pilot-scale dual fluidized-bed system," Int. Journal of Hydrogen Energy, vol. 41, no. 28, pp. 11974-11989, 2016.

[29] H. Liu, R. J. Cattolica, R. Seiser, and C.-h. Liao, "Three-dimensional full-loop simulation of a dual fluidized-bed biomass gasifier," Applied Energy, vol. 160, pp. 489-501, 2015.

[30] J. C. Bandara, R. K. Thapa, B. M. E. Moldestad, and M. S. Eikeland, "Simulation of Particle Segregation in Fluidized Beds" in 9th EUROSIM Congress on Modelling and Simulation, Oulu, Finland, 2016.

[31] R.K. Thapa, C. Pfeifer, and B. M. Halvorsen, "Modeling of reaction kinetics in bubbling fluidized bed biomass gasification reactor" Int. Journal of Energy and Environment, vol. 5, no. 1, p. 10, 2014.
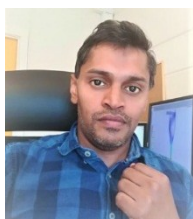
Janitha C. Bandara has completed B.Sc. degree in Chemical and Process Engineering from University of Moratuwa, Sri Lanka in 2007 and Master's degree in Process Technology from University of South-Eastern Norway in 2016. He has industrial and research experience related to biomass gasification in fixed bed and fluidized beds. At present, he is pursuing his PhD degree in experimental studies and CFD simulations of fluidized bed gasification of biomass at University of South-Eastern Norway.
E-mail address: Janitha.bandara@usn.no, janithjc@gmail.com

B.M. E. Moldestad has her Master in Process Technology from Telemark University College. The PhD degree is from Norwegian University of Science and Technology and is in the field flow behaviour in fluidized bed. Her research work includes both experimental and computational multiphase studies. She has worked within the field of fluidization since 2000. She is employed as professor at the University of South-Eastern Norway in the field Process Technology.
E-mail address: britt.moldestad@usn.no

M.S. Eikeland has her Master in Industrial Environmental Technology from Telemark University College. The PhD degree is from Norwegian University of Science and Technology and is in the field of membrane technology with focus on durability of polymer membranes exposed to aggressive gases. She has worked within the field of biomass gasification since 2014. Her research work includes both experimental and process simulation studies. She is employed as Associated Professor at University of South-Eastern Norway.
E-mail address: marianne.eikeland@usn.no